

Energy-Conserving Hermite Methods for Maxwell's Equations

Daniel Appelö¹, Thomas Hagstrom^{2*}, Yann-Meing Law³

¹Department of Mathematics, Virginia Tech, Blacksburg, 24060, VA, USA.

²Department of Mathematics, Southern Methodist University, Dallas, 75275, TX, USA.

³Department of Mathematics and Statistics, California State University Long Beach, Long Beach, 90840, CA, USA.

*Corresponding author(s). E-mail(s): thagstrom@smu.edu;
Contributing authors: appelo@vt.edu; yann-meing.law@csulb.edu;

Abstract

Energy-conserving Hermite methods for solving Maxwell's equations in dielectric and dispersive media are described and analyzed. In three space dimensions methods of order $2m$ to $2m+2$ require $(m+1)^3$ degrees-of-freedom per node for each field variable and can be explicitly marched in time with steps independent of m . We prove stability for time steps limited only by domain-of-dependence requirements along with error estimates in a special seminorm associated with the interpolation process. Numerical experiments are presented which demonstrate that Hermite methods of very high order enable the efficient simulation of electromagnetic wave propagation over thousands of wavelengths.

Keywords: Maxwell's equations, high-order methods, Hermite methods

MSC Classification: 65M70

1 Introduction

Hermite methods are general-purpose discretization schemes for solving time dependent partial differential equations exploiting the unique projection properties of

Hermite-Birkhoff interpolation [1]. Hermite methods are particularly well-suited for hyperbolic equations for two reasons:

- In contrast with typical polynomial-based element methods, Hermite methods for hyperbolic problems can march in time in interior domains with a time step, Δt , limited only by domain-of-dependence constraints, $c\Delta t \lesssim \Delta x$, independent of order.
- The cell updates require no communication with neighboring cells, and so high-order Hermite methods essentially maximize the computation-to-communication ratio.

Examples of the application of Hermite methods in the hyperbolic case include the original dissipative formulation [2] as well as more recent energy-conserving forms [3–5]. The latter references also include implementations on GPUs where the localization of the cell updates can be exploited.

Here we consider the general dispersive Maxwell system:

$$\begin{aligned}\epsilon(1 + \mathcal{K}_e^*) \frac{\partial E}{\partial t} &= \nabla \times H, \\ \mu(1 + \mathcal{K}_m^*) \frac{\partial H}{\partial t} &= -\nabla \times E.\end{aligned}$$

We assume Lorentz models for the temporal convolutions; precisely, with s the Laplace transform variable dual to time,

$$\begin{aligned}\hat{\mathcal{K}}_e &= \sum_{j=1}^{N_e} \frac{\omega_{e,j}^2}{s^2 + \gamma_{e,j}s + \Omega_{e,j}^2}, \\ \hat{\mathcal{K}}_m &= \sum_{j=1}^{N_m} \frac{\omega_{m,j}^2}{s^2 + \gamma_{m,j}s + \Omega_{m,j}^2}.\end{aligned}$$

Here we include frequency dependence not only of the permittivity but also of the permeability to account for simple homogenized models of metamaterials. Note that more general models, as discussed in [6], could also be treated, and applications of the method to nonlinear dispersive media will appear in [7]. As our focus here is on energy-conserving discretizations, we will consider cases where the dissipation can be neglected, $\gamma_{e,j} = \gamma_{m,j} = 0$, where the Lorentz model reduces to a so-called Sellmeier model. We eliminate the convolutions by introducing additional fields K_j , L_j , R_j and S_j to obtain:

$$\frac{\partial E}{\partial t} = \frac{1}{\epsilon} \nabla \times H - \sum_{j=1}^{N_e} \omega_{e,j}^2 K_j, \quad (1)$$

$$\frac{\partial K_j}{\partial t} = -\gamma_{e,j} K_j - \Omega_{e,j}^2 L_j + E, \quad (2)$$

$$\frac{\partial H}{\partial t} = -\frac{1}{\mu} \nabla \times E - \sum_{j=1}^{N_m} \omega_{m,j}^2 R_j, \quad (3)$$

$$\frac{\partial R_j}{\partial t} = -\gamma_{m,j} R_j - \Omega_{m,j}^2 S_j + H, \quad (4)$$

$$\frac{\partial L_j}{\partial t} = K_j, \quad \frac{\partial S_j}{\partial t} = R_j. \quad (5)$$

After rescaling the variables we can rewrite (1)-(5) in the form:

$$\frac{\partial V}{\partial t} = \sum_k A_k \frac{\partial W}{\partial x_k} + MW - \Gamma_V V, \quad (6)$$

$$\frac{\partial W}{\partial t} = \sum_k A_k^T \frac{\partial V}{\partial x_k} - M^T V - \Gamma_W W, \quad (7)$$

with

$$V = \begin{pmatrix} \sqrt{\epsilon} E \\ \sqrt{\epsilon} \omega_{e,1} \Omega_{e,1} L_1 \\ \vdots \\ \sqrt{\epsilon} \omega_{e,N_e} \Omega_{e,N_e} L_{N_e} \\ \sqrt{\mu} \omega_{m,1} R_1 \\ \vdots \\ \sqrt{\mu} \omega_{m,N_m} R_{N_m} \end{pmatrix}, \quad W = \begin{pmatrix} \sqrt{\mu} H \\ \sqrt{\mu} \omega_{m,1} \Omega_{m,1} S_1 \\ \vdots \\ \sqrt{\mu} \omega_{m,N_m} \Omega_{m,N_m} S_{N_m} \\ \sqrt{\epsilon} \omega_{e,1} K_1 \\ \vdots \\ \sqrt{\epsilon} \omega_{e,N_e} K_{N_e} \end{pmatrix}. \quad (8)$$

Here, in 3×3 block form, the skew-symmetric matrices A_k encode the curl operator

$$c \begin{pmatrix} \nabla \times & 0 & 0 \\ 0 & 0 & 0 \\ 0 & 0 & 0 \end{pmatrix}, \quad c = (\epsilon \mu)^{-1/2},$$

M is given by

$$M = \begin{pmatrix} 0 & 0 & -\text{diag}(\omega_{e,j}) \\ 0 & 0 & \text{diag}(\Omega_{e,j}) \\ \text{diag}(\omega_{m,j}) & -\text{diag}(\Omega_{m,j}) & 0 \end{pmatrix}.$$

and the dissipation matrices are nonnegative and diagonal,

$$\Gamma_V = \text{diag}(0 \ \gamma_{e,j} \ 0), \quad \Gamma_W = \text{diag}(0 \ \gamma_{m,j} \ 0).$$

Spatial derivatives are only applied to E and H and the characteristic speeds are c , 0 . We thus conclude that the domain-of-dependence, which is fundamental to the application of Hermite methods, is unaffected by the dispersive corrections. In addition, an energy given by $\|V\|_{L^2}^2 + \|W\|_{L^2}^2$ is conserved or dissipated (modulo boundary contributions), and the number and type of admissible boundary conditions is the same as for Maxwell's equations in a simple dielectric.

2 Conservative Hermite Discretization of the Dispersive Maxwell System

The essential ingredients of all Hermite methods are:

- i.* A cuboidal primal and dual grid,
- ii.* Degrees of freedom defined by tensor-product Taylor polynomials at the cell vertices,
- iii.* Cell polynomials constructed as tensor-product Hermite-Birkhoff interpolants of the vertex data,
- iv.* Local (cell-wise) evolution to produce updated degrees-of-freedom at dual cell nodes.

Our focus here is on energy-conserving methods exploiting the special structure of the Maxwell system. To that end we assume that $\gamma_{e,j} = \gamma_{m,j} = 0$. In our subsequent discussion we will indicate how the method can be modified to include dissipation. We note that the original dissipative Hermite method analyzed in [2] is directly applicable to the dispersive Maxwell system. However, the proposed, staggered method is more efficient and in some cases the exact energy conservation may be a desired feature. If dissipative models are used, however, the original method can be used at higher order than the method proposed here. We are assuming a uniform Cartesian mesh and piecewise uniform media. Methods for treating mapped grids to accommodate smooth boundaries are straightforward to implement and will be briefly discussed later on. We are also exploring the use of purely Cartesian meshes and embedded boundaries [8]. Denote the vertices on the primal cells by $(x_{1,j_1}, x_{2,j_2}, x_{3,j_3})$ and on the dual cells by $(x_{1,j_1+1/2}, x_{2,j_2+1/2}, x_{3,j_3+1/2})$ and set $\Delta x_k = x_{k,j_k+1} - x_{k,j_k} = x_{k,j_k+1/2} - x_{k,j_k-1/2}$.

We define V and W at different time levels and thus on different grids. Using the standard multiindex notation we define the degrees-of-freedom to be

$$V_{j_1,j_2,j_3}^{\alpha,h}(t_n) \approx \frac{\Delta x^{|\alpha|}}{\alpha!} D^\alpha V(t_n), \quad (9)$$

$$W_{j_1\pm 1/2,j_2\pm 1/2,j_3\pm 1/2}^{\alpha,h}(t_{n+1/2}) \approx \frac{\Delta x^{|\alpha|}}{\alpha!} D^\alpha W(t_{n+1/2}), \quad (10)$$

with

$$\alpha = (\alpha_1, \alpha_2, \alpha_3), \quad 0 \leq \alpha_j \leq m, \quad |\alpha| = \alpha_1 + \alpha_2 + \alpha_3.$$

To describe the numerical process assume we know $V_{j_1,j_2,j_3}^{\alpha,h}(t_n)$ and $W_{j_1\pm 1/2,j_2\pm 1/2,j_3\pm 1/2}^{\alpha,h}(t_{n+1/2})$. Our goal is to update V . The first step is to compute the tensor-product Hermite-Birkhoff interpolant of the W data. Precisely we determine the unique tensor-product vector-valued polynomial

$$\tilde{W}_{j_1,j_2,j_3}(x_1, x_2, x_3) = \sum_{k_1=0}^{2m+1} \sum_{k_2=0}^{2m+1} \sum_{k_3=0}^{2m+1} C_{k_1,k_2,k_3} (x_1 - x_{1,j_1})^{k_1} (x_2 - x_{2,j_2})^{k_2} (x_3 - x_{3,j_3})^{k_3},$$

satisfying the interpolation conditions

$$\frac{\Delta x^{|\alpha|}}{\alpha!} D^\alpha \tilde{W}_{j_1,j_2,j_3}(\mathbf{x}_{j_1\pm 1/2,j_2\pm 1/2,j_3\pm 1/2}) = W_{j_1\pm 1/2,j_2\pm 1/2,j_3\pm 1/2}^{\alpha,h}(t_{n+1/2}). \quad (11)$$

To evolve we choose q and use the Taylor approximation

$$V(t_{n+1}) = V(t_n) + 2 \sum_{\ell=1}^q \frac{(\Delta t/2)^{2\ell-1}}{(2\ell-1)!} \frac{d^{2\ell-1}V}{dt^{2\ell-1}}(t_{n+1/2}).$$

The time derivatives can be recursively computed using only \tilde{W} :

$$V^1 = \sum_k A_k \frac{\partial \tilde{W}_{j_1, j_2, j_3}}{\partial x_k} + M \tilde{W}_{j_1, j_2, j_3}, \quad (12)$$

$$V^\ell = \left(\sum_k A_k \frac{\partial}{\partial x_k} + M \right) \left(\sum_k A_k^T \frac{\partial V^{\ell-1}}{\partial x_k} - M^T V^{\ell-1} \right). \quad (13)$$

We emphasize that the functions V^ℓ are all tensor-product polynomials. Thus the updated data can be obtained by simply differentiating the temporal Taylor series in space:

$$V_{j_1, j_2, j_3}^{\alpha, h}(t_{n+1}) = V_{j_1, j_2, j_3}^{\alpha, h}(t_n) + \frac{\Delta x^{|\alpha|}}{\alpha!} D^\alpha \left(2 \sum_{\ell=1}^q \frac{(\Delta t/2)^{2\ell-1}}{(2\ell-1)!} V^\ell \right) (\mathbf{x}_{j_1, j_2, j_3}). \quad (14)$$

The procedure for updating W from $t_{n-1/2}$ to $t_{n+1/2}$ is completely analogous; we list the steps below for completeness. First compute the interpolating polynomial $\tilde{V}_{j_1+1/2, j_2+1/2, j_3+1/2}$ satisfying

$$\frac{\Delta x^{|\alpha|}}{\alpha!} D^\alpha \tilde{V}_{j_1+1/2, j_2+1/2, j_3+1/2}(\mathbf{x}_{j_1+1/2 \pm 1/2, j_2+1/2 \pm 1/2, j_3+1/2 \pm 1/2}) = V_{j_1+1/2 \pm 1/2, j_2+1/2 \pm 1/2, j_3+1/2 \pm 1/2}^{\alpha, h}(t_n). \quad (15)$$

Then compute time derivatives recursively:

$$W^1 = \sum_k A_k^T \frac{\partial \tilde{V}_{j_1+1/2, j_2+1/2, j_3+1/2}}{\partial x_k} - M^T \tilde{V}_{j_1+1/2, j_2+1/2, j_3+1/2}, \quad (16)$$

$$W^\ell = \left(\sum_k A_k^T \frac{\partial}{\partial x_k} - M^T \right) \left(\sum_k A_k \frac{\partial W^{\ell-1}}{\partial x_k} + M W^{\ell-1} \right). \quad (17)$$

Finally update the solution data:

$$W_{j_1+1/2, j_2+1/2, j_3+1/2}^{\alpha, h}(t_{n+1/2}) = W_{j_1+1/2, j_2+1/2, j_3+1/2}^{\alpha, h}(t_{n-1/2}) + \frac{\Delta x^{|\alpha|}}{\alpha!} D^\alpha \left(2 \sum_{\ell=1}^q \frac{(\Delta t/2)^{2\ell-1}}{(2\ell-1)!} W^\ell \right) (\mathbf{x}_{j_1+1/2, j_2+1/2, j_3+1/2}). \quad (18)$$

2.1 Dissipative Corrections

To include the dissipation terms in the evolution we propose solving a differential equation for these terms using an implicit Nordsieck method in predictor-corrector form [9, Ch. III-6]. For example, consider corrections to (14). Define \tilde{D}_V and $\tilde{D}_{\tilde{W}}$ as solutions to the differential equation:

$$\frac{\partial \tilde{D}_V}{\partial t} = -\Gamma_V \frac{\partial V}{\partial t}, \quad \frac{\partial \tilde{D}_{\tilde{W}}}{\partial t} = -\Gamma_W \frac{\partial \tilde{W}}{\partial t}. \quad (19)$$

Note that since the dissipation matrices are diagonal and equal to zero in many blocks these equations do not involve all the variables. In addition, since the spatial and temporal interpolation operators commute, the polynomial $\tilde{D}_{\tilde{W}}$ can be computed via the Hermite-Birkhoff spatial interpolations of polynomials computed in the preceding update of W . Maintaining the structure of (14), we must simply incorporate the additional terms in the formulas (12)-(13):

$$V^1 = \sum_k A_k \frac{\partial \tilde{W}_{j_1, j_2, j_3}}{\partial x_k} + M \tilde{W}_{j_1, j_2, j_3} + \frac{\partial \tilde{D}_{V, j_1, j_2, j_3}^{(p)}}{\partial t}, \quad (20)$$

$$V^\ell = \left(\sum_k A_k \frac{\partial}{\partial x_k} + M \right) \left(\sum_k A_k^T \frac{\partial V^{\ell-1}}{\partial x_k} - M^T V^{\ell-1} \right) + \frac{\partial^{2\ell-2} \tilde{D}_{\tilde{W}, j_1, j_2, j_3}}{\partial t^{2\ell-2}} + \frac{\partial^{2\ell-1} \tilde{D}_{V, j_1, j_2, j_3}^{(p)}}{\partial t^{2\ell-1}}. \quad (21)$$

Here we note that we are using the predicted values of \tilde{D}_V . Since the Nordsieck form represents the solution as a polynomial in time, the time derivatives can be directly computed. Also, since it is interpolated the terms involving $\tilde{D}_{\tilde{W}}$ will have the tensor-product degree $2m+1$ while \tilde{D}_V will only be of degree m . However, due to the shrinking stability domain of the Nordsieck methods with increasing p , we limit the order used to represent the dissipative terms. Therefore, the formal temporal order of the method will now be less than the spatial order for large values of m .

We remark that the implicit assumption in this procedure is that the dissipative corrections are small. Then we expect that their inclusion will have a negligible effect on the time step stability constraints. Although we exclude these terms in our analysis we include them in one of the numerical examples. We then find that in some cases the order reduction is significant and hence sometimes favors the use of lower values of m than in the nondissipative cases.

2.2 Implementation in Mapped Coordinates and Compatibility Conditions

The methods we have proposed are most efficient for piecewise uniform media. In particular the recursions (12)-(13) and (16)-(17) require significantly fewer operations when no differentiations of the coefficients are needed. At boundaries and interfaces

some modifications are required. As mentioned above, we are experimenting with embedded boundary and interface methods [8]. Although it is at this time unclear if that method can be extended to high order, it should be possible to combine it with higher order methods away from boundaries and interfaces. The alternative is to use mapped cells where necessary and to use the equations in conjunction with the interface conditions to extend the solution to ghost nodes. This approach is proposed in [10]. We note that one can choose to either define the component vectors in reference to a fixed Cartesian system or also transform them using into components referenced to the mapped system as proposed for the Yee scheme in [11]. In either case the only change to the method appears in the details of the recursions. As suggested in [10], using a representation of the mapping as a Taylor polynomial of sufficiently high order centered in the cell, the additional cost involves the multiplication of the derivatives of the field interpolants by the coefficients arising from the mapping. For example

$$\frac{\partial V}{\partial x_k} = \sum_j \frac{\partial r_j}{\partial x_k} \frac{\partial V}{\partial r_j},$$

increasing the cost due to the three polynomial multiplications. Note that these multiplications can be truncated according to the eventual truncation of the update.

The major complication in the implementation of Hermite methods is the imposition of boundary and interface conditions. This stems from the need to provide normal derivative data to update the solution in the cells adjacent to the boundary. For the dissipative formulation three approaches have had success:

- i.* Coupling with discontinuous Galerkin discretizations in a possibly unstructured mesh near the boundary [12]. Here local time stepping in the DG elements allows us to retain the large global time steps in most of the domain.
- ii.* The correction function method [13]. This involves a weighted least-squares construction of a space-time polynomial near the boundary. Penalty terms in the least squares construction involve the boundary evolution, Maxwell's equations, and a match with the Hermite evolution in nearby volume cells.
- iii.* Compatibility conditions [10]. Here one uses the boundary conditions along with the equation and its normal and tangential derivatives to compute the missing data required to evolve the polynomial at the boundary.

Of these methods, only the compatibility approach has been demonstrated to work with a conservative Hermite method, namely the scheme for the scalar wave equation studied in [3]. As such it is not directly applicable to the Maxwell system studied here, though it is a promising avenue of future research to explore its extension to the present case. Consider the example of a flat PEC boundary $x_1 = \text{constant}$. Then if the mesh containing the magnetic field is aligned with the boundary the problem is to determine the electric field and its derivatives at a dual ghost node. This is easily accomplished by assuming that the tangential fields are extended as odd functions and the normal field as an even function. Extending this procedure to a curved boundary and mapped coordinates leads to an algebraic system enforcing a zero tangential field along the boundary and a zero normal derivative of the projection of the electric field

in the normal direction. In [10] the scalar wave equation is considered and sixth order convergence for a conservative Hermite scheme with $m = 3$ is demonstrated.

3 Stability and Convergence

To establish the stability and convergence of the proposed method we exploit the projection property of the Hermite-Birkhoff interpolation process defined by (11), (15) along with standard interpolation error estimates. (See [2–4] for detailed proofs.) We will assume throughout this section that the solution is 2π -periodic in each Cartesian coordinate and denote the domain by \mathbb{T} . Denote by \mathcal{I}_m the interpolation operator; to cut down on the required notation we use the same symbol for interpolation on the dual and primal grids. The essential property is expressed as the orthogonality of interpolants and interpolation errors in a certain seminorm, which we will call the HB seminorm. Precisely, if we define for any vector functions f and g the semi-inner-product

$$\langle f, g \rangle_m = \left\langle \frac{\partial^{3m+3} f}{\partial x_1^{m+1} \partial x_2^{m+1} \partial x_3^{m+1}}, \frac{\partial^{3m+3} g}{\partial x_1^{m+1} \partial x_2^{m+1} \partial x_3^{m+1}} \right\rangle_{(L^2(\mathbb{T}))^3}, \quad (22)$$

then

$$\langle \mathcal{I}_m f, g - \mathcal{I}_m g \rangle_m = 0. \quad (23)$$

Denoting by $|\cdot|_m^2$ the seminorm associated with the semi-inner-product (23) implies the Pythagorean Theorem:

$$|f|_m^2 = |\mathcal{I}_m f|_m^2 + |f - \mathcal{I}_m f|_m^2. \quad (24)$$

We will focus on establishing stability and convergence for the case of a dielectric medium. Since the dispersive terms present themselves as zero order perturbations to the dielectric system they are straightforward to include, at least suboptimally, once the principal order terms have been handled. The time-staggered exact evolution satisfies an energy conservation law in any Sobolev seminorm, including the HB seminorm defined above. Expanding in a Fourier series in space, let $\hat{E}(k, t)$, $\hat{H}(k, t)$ be the Fourier coefficients of the symmetrized variables $\tilde{E} = \sqrt{\epsilon}E$, $\tilde{H} = \sqrt{\mu}H$. They satisfy the ordinary differential equations

$$\frac{\partial \hat{E}}{\partial t} = ick \times \hat{H}, \quad \frac{\partial \hat{H}}{\partial t} = -ick \times \hat{E}. \quad (25)$$

For $k \neq 0$ set $k = |k|\hat{k}$. We will make use of an orthogonal decomposition of the fields $\tilde{E} = E_S + E_N$, $\tilde{H} = H_S + H_N$ defined for any vector function U by:

$$\widehat{U}_N(k) = \hat{k}\hat{k}^T \hat{U}(k), \quad \widehat{U}_S(k) = \hat{U}(k) - \widehat{U}_N(k). \quad (26)$$

We also define the operator \mathcal{C} applied to any vector function U by

$$\widehat{\mathcal{C}U}(k) = \hat{k} \times \hat{U}(k), \quad (27)$$

and note the identities which follow from elementary identities satisfied by the cross product

$$\mathcal{C}U = \mathcal{C}U_S, \quad \mathcal{C}^2U_S = -U_S, \quad \left| \widehat{\mathcal{C}U_S}(k) \right| = \left| \widehat{U_S}(k) \right|. \quad (28)$$

The last identity combined with Parseval's relation implies that \mathcal{C} preserves all Sobolev norms of U_S .

We also define operators S_{\pm} as in [3, 4]:

$$\widehat{S^{\pm}U}(k) = e^{\pm ic|k|\Delta t/2} \widehat{U}(k), \quad (29)$$

noting that $S^- = S^{+,*}$ and that the operators are unitary,

$$S^+S^- = S^-S^+ = I. \quad (30)$$

In addition they commute with the operator \mathcal{C} . Then the exact evolution formulas take the form:

$$\tilde{E}(\mathbf{x}, t + \Delta t) = \tilde{E}(\mathbf{x}, t) + (S^+ - S^-) \mathcal{C} \tilde{H}(\mathbf{x}, t + \Delta t/2), \quad (31)$$

$$\tilde{H}(\mathbf{x}, t + \Delta t/2) = \tilde{H}(\mathbf{x}, t - \Delta t/2) - (S^+ - S^-) \mathcal{C} \tilde{E}(\mathbf{x}, t). \quad (32)$$

Rewriting these in terms of the orthogonal decomposition and utilizing (28) we have

$$E_S(\mathbf{x}, t + \Delta t) = E_S(\mathbf{x}, t) + (S^+ - S^-) \mathcal{C} H_S(\mathbf{x}, t + \Delta t/2), \quad (33)$$

$$H_S(\mathbf{x}, t + \Delta t/2) = H_S(\mathbf{x}, t - \Delta t/2) - (S^+ - S^-) \mathcal{C} E_S(\mathbf{x}, t), \quad (34)$$

$$E_N(\mathbf{x}, t + \Delta t) = E_N(\mathbf{x}, t), \quad (35)$$

$$H_N(\mathbf{x}, t + \Delta t/2) = H_N(\mathbf{x}, t - \Delta t/2). \quad (36)$$

Assuming $\nabla \cdot E = \nabla \cdot H = 0$ initially equations (35)-(36) simply imply that the fields will be solenoidal at all subsequent discrete times. We will assume this to be true when estimating the errors. Setting

$$P^{\pm}(\mathbf{x}, t) = E_S(\mathbf{x}, t) \mp S^{\pm} \mathcal{C} H_S(\mathbf{x}, t - \Delta t/2), \quad (37)$$

$$Q^{\pm}(\mathbf{x}, t + \Delta t/2) = H_S(\mathbf{x}, t + \Delta t/2) \pm S^{\pm} \mathcal{C} E_S(\mathbf{x}, t), \quad (38)$$

and using (28) and (30) again we rewrite the evolution formulas (33)-(34):

$$\begin{aligned} P^+(\mathbf{x}, t + \Delta t) &= -S^- \mathcal{C} Q^+(\mathbf{x}, t + \Delta t/2), \\ P^-(\mathbf{x}, t + \Delta t) &= S^+ \mathcal{C} Q^-(\mathbf{x}, t + \Delta t/2), \end{aligned} \quad (39)$$

$$\begin{aligned} Q^+(\mathbf{x}, t + \Delta t/2) &= S^- \mathcal{C} P^+(\mathbf{x}, t), \\ Q^-(\mathbf{x}, t + \Delta t/2) &= -S^+ \mathcal{C} P^-(\mathbf{x}, t). \end{aligned} \quad (40)$$

By the norm preserving properties of the operators S^\pm and \mathcal{C} we deduce the basic conservation laws in any Sobolev norm or seminorm

$$\|P^\pm(\cdot, t + \Delta t)\| = \|Q^\pm(\cdot, t + \Delta t/2)\| = \|P^\pm(\cdot, t)\|. \quad (41)$$

We now note that for polynomial data the recursions (13), (17) will terminate once the number of spatial derivatives exceeds the degree. For the tensor-product polynomials of total degree $6m + 3$ we are using we have

$$V_\ell = W_\ell = 0, \quad \ell > 3m + 2.$$

Thus if we take $q = 3m + 2$ the cell polynomials are evolved exactly. Moreover, if we obey the CFL restriction

$$c\Delta t < \max_k \Delta x_k, \quad (42)$$

then we have the following lemma. Here we define \tilde{E}^h, \tilde{H}^h to be the Hermite-Birkhoff interpolants of the vertex data and define the quantities $P^{\pm,h}, Q^{\pm,h}$ as in (37).

Lemma 1. *For the dielectric system, $M = \Gamma_V = \Gamma_W = 0$, if $q = 3m + 2$ and (42) holds then the quantities $P^{\pm,h}, E_N^h, Q^{\pm,h}$ and H_N^h computed from the approximations, \tilde{E}^h, \tilde{H}^h , to the symmetrized variables satisfy the evolution formulas:*

$$\begin{aligned} & P^{+,h}(\mathbf{x}, t + \Delta t) + E_N^h(\mathbf{x}, t + \Delta t) = \\ & -\mathcal{I}_m (S^- \mathcal{C} Q^{+,h}(\mathbf{x}, t + \Delta t/2) - E_N^h(\mathbf{x}, t)) \\ & -(1 - \mathcal{I}_m) (S^+ \mathcal{C} Q^{-,h}(\mathbf{x}, t + \Delta t/2) + E_N^h(\mathbf{x}, t)), \\ & P^{-,h}(\mathbf{x}, t + \Delta t) + E_N^h(\mathbf{x}, t + \Delta t) = \\ & \mathcal{I}_m (S^+ \mathcal{C} Q^{-,h}(\mathbf{x}, t + \Delta t/2) + E_N^h(\mathbf{x}, t)) \\ & +(1 - \mathcal{I}_m) (S^- \mathcal{C} Q^{+,h}(\mathbf{x}, t + \Delta t/2) - E_N^h(\mathbf{x}, t)), \\ & Q^{+,h}(\mathbf{x}, t + \Delta t/2) + H_N^h(\mathbf{x}, t + \Delta t/2) = \\ & \mathcal{I}_m (S^- \mathcal{C} P^{+,h}(\mathbf{x}, t) + H_N^h(\mathbf{x}, t + \Delta t/2)) \\ & +(1 - \mathcal{I}_m) (S^+ \mathcal{C} Q^{-,h}(\mathbf{x}, t + \Delta t/2) - H_N^h(\mathbf{x}, t - \Delta t/2)), \\ & Q^{-,h}(\mathbf{x}, t + \Delta t/2) + H_N^h(\mathbf{x}, t + \Delta t/2) = \\ & -\mathcal{I}_m (S^+ \mathcal{C} P^{-,h}(\mathbf{x}, t) - H_N^h(\mathbf{x}, t - \Delta t/2)) \\ & -(1 - \mathcal{I}_m) (S^- \mathcal{C} P^{+,h}(\mathbf{x}, t) + H_N^h(\mathbf{x}, t - \Delta t/2)). \end{aligned} \quad (43)$$

Proof. Assuming (42), the domain of dependence of the solution at the cell centers on either grid lies completely within the cell. Therefore, since the cell polynomial is updated exactly if we take $q = 3m + 2$, the data used to compute the Hermite-Birkhoff interpolants is the exact evolution of the approximate solution at the previous times. Thus the only error over a time step is the interpolation error which can then be projected onto the various solution components. The further complications in the formulas (43) in comparison to (39) arise from the fact that the projections do not commute with \mathcal{I}_m . Recalling that \mathcal{I}_m is a projection the discrete evolution formulas

are

$$\tilde{E}^h(\mathbf{x}, t + \Delta t) = \tilde{E}^h(\mathbf{x}, t) + \mathcal{I}_m (S^+ - S^-) H_S^h(\mathbf{x}, t + \Delta t/2), \quad (44)$$

$$\tilde{H}^h(\mathbf{x}, t + \Delta t/2) = \tilde{H}^h(\mathbf{x}, t - \Delta t/2) - \mathcal{I}_m (S^+ - S^-) E_S^h(\mathbf{x}, t). \quad (45)$$

Consider, for example, the update formula for $P^{+,h} + E_N^h$ making use of (44)-(45) along with (28) and (30). Note that

$$\tilde{E}^h(\mathbf{x}, t) = \mathcal{I}_m \tilde{E}^h(\mathbf{x}, t) = -\mathcal{I}_m S^- \mathcal{C} S^+ \mathcal{C} E_S^h(\mathbf{x}, t) + \mathcal{I}_m E_N^h(\mathbf{x}, t),$$

$$0 = -(1 - \mathcal{I}_m) \tilde{E}^h(\mathbf{x}, t) = (1 - \mathcal{I}_m) S^+ \mathcal{C} S^- \mathcal{C} E_S^h(\mathbf{x}, t) - (1 - \mathcal{I}_m) E_N^h(\mathbf{x}, t).$$

We compute

$$\begin{aligned} P^{+,h}(\mathbf{x}, t + \Delta t) + E_N^h(\mathbf{x}, t + \Delta t) &= \\ \tilde{E}^h(\mathbf{x}, t + \Delta t) - S^+ \mathcal{C} H_S^h(\mathbf{x}, t + \Delta t/2) &= \\ -\mathcal{I}_m (S^- \mathcal{C} (H_S^h(\mathbf{x}, t + \Delta t/2) + S^+ \mathcal{C} E_S^h(\mathbf{x}, t)) - E_N^h(\mathbf{x}, t)) &= \\ -(1 - \mathcal{I}_m) (S^+ \mathcal{C} (H_S^h(\mathbf{x}, t + \Delta t/2) - S^- \mathcal{C} E_S^h(\mathbf{x}, t)) + E_N^h(\mathbf{x}, t)) &= \\ -\mathcal{I}_m (S^- \mathcal{C} Q^{+,h}(\mathbf{x}, t + \Delta t/2) - E_N^h(\mathbf{x}, t)) &= \\ -(1 - \mathcal{I}_m) (S^+ \mathcal{C} Q^{-,h}(\mathbf{x}, t + \Delta t/2) + E_N^h(\mathbf{x}, t)). & \end{aligned}$$

The other identities in (43) are similarly derived. \square

We are now in a position to prove Theorem 1.

Theorem 1. *For the dielectric system, $M = \Gamma_V = \Gamma_W = 0$, if $q = 3m + 2$ and (42) holds then the approximate solution satisfies the conservation laws*

$$\begin{aligned} &|P^{+,h}(\cdot, t + \Delta t)|_m^2 + |P^{-,h}(\cdot, t + \Delta t)|_m^2 \\ &+ 2 |E_N^h(\cdot, t + \Delta t)|_m^2 + 2 |H_N^h(t + \Delta t/2)|_m^2 = \\ &|Q^{+,h}(\cdot, t + \Delta t/2)|_m^2 + |Q^{-,h}(\cdot, t + \Delta t/2)|_m^2 \quad (46) \\ &+ 2 |H_N^h(\cdot, t + \Delta t/2)|_m^2 + 2 |E_N^h(t)|_m^2 = \\ &|P^{+,h}(\cdot, t)|_m^2 + |P^{-,h}(\cdot, t)|_m^2 + 2 |E_N^h(\cdot, t)|_m^2 + 2 |H_N^h(t - \Delta t/2)|_m^2. \end{aligned}$$

Proof. Compute recalling the fact that $P^{\pm,h}$ and $Q^{\pm,h}$ are orthogonal to $E^{N,h}$ and $H^{N,h}$ in the HB semi-inner product.

$$\begin{aligned} &|P^{+,h}(\cdot, t + \Delta t)|_m^2 + |E_N^h(\cdot, t + \Delta t)|_m^2 = \\ &|P^{+,h}(\cdot, t + \Delta t) + E_N^h(\cdot, t + \Delta t)|_m^2 = \\ &|\mathcal{I}_m (S^- \mathcal{C} Q^{+,h}(\mathbf{x}, t + \Delta t/2) - E_N^h(\mathbf{x}, t))|_m^2 \\ &+ |(1 - \mathcal{I}_m) (S^+ \mathcal{C} Q^{-,h}(\mathbf{x}, t + \Delta t/2) + E_N^h(\mathbf{x}, t))|_m^2 = \end{aligned}$$

$$\begin{aligned}
& \left| \mathcal{I}_m S^- \mathcal{C} Q^{+,h}(\mathbf{x}, t + \Delta t/2) \right|_m^2 \\
& + \left| (1 - \mathcal{I}_m) S^+ \mathcal{C} Q^{-,h}(\mathbf{x}, t + \Delta t/2) \right|_m^2 + \left| E_N^h(\mathbf{x}, t) \right|_m^2 \\
& \quad - 2 \langle \mathcal{I}_m S^- \mathcal{C} Q^{+,h}(\mathbf{x}, t + \Delta t/2), \mathcal{I}_m E_N^h(\mathbf{x}, t) \rangle_m \\
& + 2 \langle (1 - \mathcal{I}_m) S^+ \mathcal{C} Q^{-,h}(\mathbf{x}, t + \Delta t/2), (1 - \mathcal{I}_m) E_N^h(\mathbf{x}, t) \rangle_m.
\end{aligned}$$

$$\begin{aligned}
& \left| P^{-,h}(\cdot, t + \Delta t) \right|_m^2 + \left| E_N^h(\cdot, t + \Delta t) \right|_m^2 = \\
& \quad \left| P^{-,h}(\cdot, t + \Delta t) + E_N^h(\cdot, t + \Delta t) \right|_m^2 = \\
& \quad \left| \mathcal{I}_m (S^+ \mathcal{C} Q^{-,h}(\mathbf{x}, t + \Delta t/2) + E_N^h(\mathbf{x}, t)) \right|_m^2 \\
& + \left| (1 - \mathcal{I}_m) (S^- \mathcal{C} Q^{+,h}(\mathbf{x}, t + \Delta t/2) - E_N^h(\mathbf{x}, t)) \right|_m^2 = \\
& \quad \left| \mathcal{I}_m S^+ \mathcal{C} Q^{-,h}(\mathbf{x}, t + \Delta t/2) \right|_m^2 \\
& + \left| (1 - \mathcal{I}_m) S^- \mathcal{C} Q^{+,h}(\mathbf{x}, t + \Delta t/2) \right|_m^2 + \left| E_N^h(\mathbf{x}, t) \right|_m^2 \\
& \quad + 2 \langle \mathcal{I}_m S^+ \mathcal{C} Q^{-,h}(\mathbf{x}, t + \Delta t/2), \mathcal{I}_m E_N^h(\mathbf{x}, t) \rangle_m \\
& - 2 \langle (1 - \mathcal{I}_m) S^- \mathcal{C} Q^{+,h}(\mathbf{x}, t + \Delta t/2), (1 - \mathcal{I}_m) E_N^h(\mathbf{x}, t) \rangle_m.
\end{aligned}$$

Adding these expressions we find

$$\begin{aligned}
& \left| P^{+,h}(\cdot, t + \Delta t) \right|_m^2 + \left| P^{-,h}(\cdot, t + \Delta t) \right|_m^2 + 2 \left| E_N^h(\cdot, t + \Delta t) \right|_m^2 = \\
& \left| S^- \mathcal{C} Q^{+,h}(\mathbf{x}, t + \Delta t/2) \right|_m^2 + \left| S^+ \mathcal{C} Q^{-,h}(\mathbf{x}, t + \Delta t/2) \right|_m^2 + 2 \left| E_N^h(\mathbf{x}, t) \right|_m^2 \\
& \quad - 2 \langle \mathcal{I}_m S^- \mathcal{C} Q^{+,h}(\mathbf{x}, t + \Delta t/2), \mathcal{I}_m E_N^h(\mathbf{x}, t) \rangle_m \\
& \quad - 2 \langle (1 - \mathcal{I}_m) S^+ \mathcal{C} Q^{-,h}(\mathbf{x}, t + \Delta t/2), (1 - \mathcal{I}_m) E_N^h(\mathbf{x}, t) \rangle_m \\
& \quad + 2 \langle (1 - \mathcal{I}_m) S^+ \mathcal{C} Q^{-,h}(\mathbf{x}, t + \Delta t/2), (1 - \mathcal{I}_m) E_N^h(\mathbf{x}, t) \rangle_m \\
& \quad + 2 \langle \mathcal{I}_m S^+ \mathcal{C} Q^{-,h}(\mathbf{x}, t + \Delta t/2), \mathcal{I}_m E_N^h(\mathbf{x}, t) \rangle_m = \\
& \left| Q^{+,h}(\mathbf{x}, t + \Delta t/2) \right|_m^2 + \left| Q^{-,h}(\mathbf{x}, t + \Delta t/2) \right|_m^2 + 2 \left| E_N^h(\mathbf{x}, t) \right|_m^2 \\
& \quad - 2 \langle Q^{+,h}(\mathbf{x}, t + \Delta t/2), E_N^h(\mathbf{x}, t) \rangle_m \\
& \quad + 2 \langle Q^{-,h}(\mathbf{x}, t + \Delta t/2), E_N^h(\mathbf{x}, t) \rangle_m = \\
& \left| Q^{+,h}(\mathbf{x}, t + \Delta t/2) \right|_m^2 + \left| Q^{-,h}(\mathbf{x}, t + \Delta t/2) \right|_m^2 + 2 \left| E_N^h(\mathbf{x}, t) \right|_m^2.
\end{aligned}$$

Adding $2 \left| H_N^h(t + \Delta t/2) \right|_m^2$ to both sides of this equation yields the first equality in (46). The second is proven similarly using the update formulas for $Q^{\pm,h}$ in (43). \square

Having established stability we move on to derive error estimates. To this end it is useful to organize the previous results in terms of the evolution of the conserved

quantities. Specifically we introduce the HB-seminorm conserving operators \mathcal{U} and \mathcal{V} :

$$\begin{pmatrix} P^{+,h}(\mathbf{x}, t + \Delta t) \\ P^{-,h}(\mathbf{x}, t + \Delta t) \\ E_N^h(\mathbf{x}, t + \Delta t) \\ H_N^h(\mathbf{x}, t + \Delta t/2) \end{pmatrix} = \mathcal{U}^h \begin{pmatrix} Q^{+,h}(\mathbf{x}, t + \Delta t/2) \\ Q^{-,h}(\mathbf{x}, t + \Delta t/2) \\ H_N^h(\mathbf{x}, t + \Delta t/2) \\ E_N^h(\mathbf{x}, t) \end{pmatrix}, \quad (47)$$

$$\begin{pmatrix} Q^{+,h}(\mathbf{x}, t + \Delta t/2) \\ Q^{-,h}(\mathbf{x}, t + \Delta t/2) \\ H_N^h(\mathbf{x}, t + \Delta t/2) \\ E_N^h(\mathbf{x}, t) \end{pmatrix} = \mathcal{V}^h \begin{pmatrix} P^{+,h}(\mathbf{x}, t) \\ P^{-,h}(\mathbf{x}, t) \\ E_N^h(\mathbf{x}, t) \\ H_N^h(\mathbf{x}, t - \Delta t/2) \end{pmatrix}. \quad (48)$$

Define errors in the conserved quantities by

$$\mathcal{E}(t_n) = \begin{pmatrix} P^+(\mathbf{x}, t_n) - P^{+,h}(\mathbf{x}, t_n) \\ P^-(\mathbf{x}, t_n) - P^{-,h}(\mathbf{x}, t_n) \\ E_N(\mathbf{x}, t_n) - E_N^h(\mathbf{x}, t_n) \\ H_N(\mathbf{x}, t_{n-1/2}) - H_N^h(\mathbf{x}, t_{n-1/2}) \end{pmatrix}, \quad (49)$$

$$\mathcal{E}(t_{n+1/2}) = \begin{pmatrix} Q^+(\mathbf{x}, t_{n+1/2}) - Q^{+,h}(\mathbf{x}, t_{n+1/2}) \\ Q^-(\mathbf{x}, t_{n+1/2}) - Q^{-,h}(\mathbf{x}, t_{n+1/2}) \\ H_N(\mathbf{x}, t_{n+1/2}) - H_N^h(\mathbf{x}, t_{n+1/2}) \\ E_N(\mathbf{x}, t_n) - E_N^h(\mathbf{x}, t_n) \end{pmatrix}, \quad (50)$$

where we have introduced $t_n = n\Delta t$, $t_{n+1/2} = (n + 1/2)\Delta t$. Convergence in the HB seminorm is established in Theorem 2

Theorem 2. *For the dielectric system, $M = \Gamma_V = \Gamma_W = 0$, if $q = 3m + 2$, the CFL number $\frac{\Delta t}{h}$ is fixed and satisfies (42), and the initial approximations are sufficiently accurate, there exists C depending only on m , the CFL number, and derivatives of the solution $\tilde{E}(\mathbf{x}, t)$, $\tilde{H}(\mathbf{x}, t)$, such that, for $h = \max(h_x, h_y, h_z)$*

$$|\mathcal{E}(t_n)|_m + |\mathcal{E}(t_{n+1/2})|_m \leq C(1 + t_n)h^{m+1}. \quad (51)$$

Proof. We combine (43) with the exact formulas (33)-(36) to derive evolution formulas for \mathcal{E} . We begin with the first two equations. Note that we are assuming $E_N = 0$ and $H_N = 0$ but for clarity we retain them in the error equations.

$$\begin{aligned} & P^+(\mathbf{x}, t_{n+1}) - P^{+,h}(\mathbf{x}, t_{n+1}) + E_N(\mathbf{x}, t_{n+1}) - E_N^h(\mathbf{x}, t_{n+1}) = \\ & -\mathcal{I}_m (S^- \mathcal{C} (Q^+(\mathbf{x}, t_{n+1/2}) - Q^{+,h}(\mathbf{x}, t_{n+1/2})) - (E_N(\mathbf{x}, t_{n+1}) - E_N^h(\mathbf{x}, t_n))) \\ & -(1 - \mathcal{I}_m) (S^+ \mathcal{C} (Q^-(\mathbf{x}, t_{n+1/2}) - Q^{-,h}(\mathbf{x}, t_{n+1/2})) + (E_N(\mathbf{x}, t_n) - E_N^h(\mathbf{x}, t_n))) \\ & \quad + (1 - \mathcal{I}_m) (E_S(\mathbf{x}, t_{n+1}) - E_S(\mathbf{x}, t_n)), \end{aligned}$$

$$\begin{aligned} & P^-(\mathbf{x}, t_{n+1}) - P^{-,h}(\mathbf{x}, t_n) + E_N(\mathbf{x}, t_{n+1}) - E_N^h(\mathbf{x}, t_{n+1}) = \\ & +\mathcal{I}_m (S^+ \mathcal{C} (Q^-(\mathbf{x}, t_{n+1/2}) - Q^{-,h}(\mathbf{x}, t_{n+1/2})) + (E_N(\mathbf{x}, t_{n+1}) - E_N^h(\mathbf{x}, t_n))) \\ & +(1 - \mathcal{I}_m) (S^- \mathcal{C} (Q^+(\mathbf{x}, t_{n+1/2}) - Q^{+,h}(\mathbf{x}, t_{n+1/2})) - (E_N(\mathbf{x}, t_n) - E_N^h(\mathbf{x}, t_n))) \end{aligned}$$

$$+(1 - \mathcal{I}_m) (E_S(\mathbf{x}, t_{n+1}) - E_S(\mathbf{x}, t_n)).$$

Similarly we can write down the evolution of the error for E_N

$$\begin{aligned} E_N(\mathbf{x}, t_{n+1}) - E_N^h(\mathbf{x}, t_{n+1}) &= N\mathcal{I}_m (S^+ - S^-) \mathcal{C} (H_S(\mathbf{x}, t_{n+1/2}) - H_S^h(\mathbf{x}, t_{n+1/2})) \\ &\quad + N(1 - \mathcal{I}_m) (E_S(\mathbf{x}, t_{n+1}) - E_S(\mathbf{x}, t_n)). \end{aligned}$$

Note that the H_N error is simply copied in this step of the evolution. We can rewrite these relations as

$$\mathcal{E}(t_{n+1}) = \mathcal{U}^h \mathcal{E}(t_{n+1/2}) + \tau_{n+1}$$

where

$$\tau_{n+1} = \begin{pmatrix} [(1 - \mathcal{I}_m) (E_S(\mathbf{x}, t_{n+1}) - E_S(\mathbf{x}, t_n))]_S \\ [(1 - \mathcal{I}_m) (E_S(\mathbf{x}, t_{n+1}) - E_S(\mathbf{x}, t_n))]_S \\ [(1 - \mathcal{I}_m) (E_S(\mathbf{x}, t_{n+1}) - E_S(\mathbf{x}, t_n))]_N \\ 0 \end{pmatrix}.$$

Assuming a smooth solution to the continuous problem the standard Hermite-Birkhoff interpolation error formulas (e.g [2]) imply:

$$|(1 - \mathcal{I}_m) (E_S(\mathbf{x}, t_{n+1}) - E_S(\mathbf{x}, t_n))|_m \leq C \frac{\Delta t}{2} h^{m+1}.$$

So invoking the triangle inequality for the seminorm and the fact that \mathcal{U}^h preserves the seminorm we have

$$|\mathcal{E}(t_{n+1})|_m \leq |\mathcal{U}^h \mathcal{E}(t_{n+1/2})|_m + |\tau_{n+1}|_m \leq |\mathcal{E}(t_{n+1/2})|_m + C \frac{\Delta t}{2} h^{m+1}.$$

By similar computations we deduce

$$|\mathcal{E}(t_{n+1/2})|_m \leq |\mathcal{E}(t_n)|_m + C \frac{\Delta t}{2} h^{m+1}.$$

Summing these inequalities we have

$$|\mathcal{E}(t_n)|_m + |\mathcal{E}(t_{n+1/2})|_m \leq |\mathcal{E}(t_0)|_m + |\mathcal{E}(t_{1/2})|_m + C t_n h^{m+1}.$$

Assuming, as would be the case if we interpolate a smooth initial condition and initial half-step,

$$|\mathcal{E}(t_0)|_m \leq C h^{m+1}, \quad |\mathcal{E}(t_{1/2})|_m \leq C h^{m+1},$$

we obtain the final result. □

3.1 Extensions to the Dispersive System

Inclusion of the dispersive terms does not change the domain-of-dependence of the exact solution. Thus, excluding the dissipative terms, we believe that the previous

analysis could be repeated via the definition of the complex exponentials of the operators appearing in the update formulas. However, we can no longer expect to evolve the cell polynomials exactly and so need to take account of additional sources of error. Therefore we will follow the standard analysis of stability for leap-frog schemes as presented in [14]. Again ignoring the dissipative term and using the fact that \mathcal{I}_m is a projection we can write the discrete evolution equations (14), (18), in the form:

$$\begin{aligned} V(\mathbf{x}, t_{n+1}) - V(\mathbf{x}, t_n) &= \mathcal{I}_m \mathcal{B} \mathcal{I}_m W(\mathbf{x}, t_{n+1/2}), \\ W(\mathbf{x}, t_{n+1/2}) - W(\mathbf{x}, t_{n-1/2}) &= -\mathcal{I}_m \mathcal{B}^* \mathcal{I}_m V(\mathbf{x}, t_n), \end{aligned}$$

where

$$\mathcal{B} \mathcal{I}_m W = \sum_{\ell=1}^q \frac{(\Delta t/2)^{2\ell-1}}{(2\ell-1)!} V^\ell, \quad (52)$$

with V^ℓ defined by (12)-(13). Now consider the scaling of terms in (12)-(13). When restricted to the polynomial space the derivative operators $\frac{\partial}{\partial x_k} \propto \Delta x_k^{-1}$. Therefore, for fixed CFL numbers, $\lambda_k = c\Delta t/\Delta x_k$, we have

$$\mathcal{I}_m \mathcal{B} \mathcal{I}_m = \mathcal{I}_m (\mathcal{B}_0 + \Delta t \mathcal{B}_1) \mathcal{I}_m, \quad (53)$$

where \mathcal{B}_0 is independent of Δt and \mathcal{B}_1 is bounded. In particular \mathcal{B}_0 is the evolution operator for the dielectric case combined with some additional zero blocks.

We then have Theorem 3 and conditional stability follows.

Theorem 3. *For the conservative system, $\Gamma_V = \Gamma_W = 0$, the following quantities are constant:*

$$|V(\cdot, t_n)|_m^2 + \frac{1}{4} |W(\cdot, t_{n+1/2}) + W(\cdot, t_{n-1/2})|_m^2 - \frac{1}{4} |\mathcal{I}_m \mathcal{B}^* V(\cdot, t_n)|_m^2, \quad (54)$$

$$|W(\cdot, t_{n+1/2})|_m^2 + \frac{1}{4} |V(\cdot, t_{n+1}) + V(\cdot, t_n)|_m^2 - \frac{1}{4} |\mathcal{I}_m \mathcal{B}^* W(\cdot, t_{n+1/2})|_m^2. \quad (55)$$

Corollary 1. *For the conservative system, $\Gamma_V = \Gamma_W = 0$, we have stability in the HB seminorm if*

$$\|\mathcal{B}\|_m < 4, \quad \|\mathcal{B}^*\|_m < 4. \quad (56)$$

Remark 1. *Condition (56) plays the role of a CFL condition. Invoking (53) and Theorem 1 and taking $q = 3m + 2$ we expect stability for Δt small enough under the domain-of-dependence CFL condition (42). In our experiments we find that the method is stable in both the dielectric and dispersive case with large CFL numbers and smaller values of q .*

Proof. Combining two steps in (18) we have the formula

$$W(\mathbf{x}, t_{n+3/2}) - W(\mathbf{x}, t_{n-1/2}) = -\mathcal{I}_m \mathcal{B}^* \mathcal{I}_m (V(\mathbf{x}, t_{n+1}) + V(\mathbf{x}, t_n)).$$

Taking the HB inner product of this equation with $W(\mathbf{x}, t_{n+3/2})$ and the HB inner product of (14) with $V(\mathbf{x}, t_{n+1}) + V(\mathbf{x}, t_n)$ we obtain

$$\langle W(\cdot, t_{n+3/2}), W(\cdot, t_{n+1/2}) \rangle_m = \langle W(\cdot, t_{n+1/2}), W(\cdot, t_{n-1/2}) \rangle_m$$

$$-\langle W(\cdot, t_{n+1/2}), \mathcal{I}_m \mathcal{B}^* \mathcal{I}_m (V(\cdot, t_{n+1}) + V(\cdot, t_n)) \rangle_m,$$

$$|V(\cdot, t_{n+1})|_m^2 = |V(\cdot, t_n)|_m^2 + \langle \mathcal{I}_m \mathcal{B} \mathcal{I}_m W(\cdot, t_{n+1/2}), V(\cdot, t_{n+1}) + V(\cdot, t_n) \rangle_m.$$

Adding these expressions and noting that the terms involving \mathcal{B} and \mathcal{B}^* cancel we deduce that the quantity

$$|V(\cdot, t_n)|_m^2 + \langle W(\cdot, t_{n+1/2}), W(\cdot, t_{n-1/2}) \rangle_m$$

is constant. We rewrite the second term by noting that

$$\begin{aligned} \frac{1}{4} |W(\cdot, t_{n+1/2}) + W(\cdot, t_{n-1/2})|_m^2 - \frac{1}{4} |W(\cdot, t_{n+1/2}) - W(\cdot, t_{n-1/2})|_m^2 = \\ \langle W(\cdot, t_{n+1/2}), W(\cdot, t_{n-1/2}) \rangle_m. \end{aligned}$$

Replacing the difference term with (18) yields (54). Equation (55) is derived by the analogous procedure. \square

Given the stability Theorem, error estimates in the HB seminorm can also be obtained by standard means. We will not present them here, but instead focus on observing stability bounds and convergence rates in L^2 in numerical experiments. One can attempt a standard analysis of convergence by studying the local truncation error method and the associated stability of the scheme. The approximation of derivatives by the Hermite interpolant of a smooth function at the cell centers will have errors which scale with $|\Delta x|^{2m+2-j}$ for derivatives of even order and $|\Delta x|^{2m+3-j}$ for derivatives of odd order. Therefore, if we consider the evolution of the scaled discrete data (9)-(10) and take $q \geq m$ we derive estimates of the local truncation error of order $\Delta t |\Delta x|^{2m+2}$ for even derivatives and $\Delta t |\Delta x|^{2m+1}$ for odd derivatives. However, translating stability from the HB-seminorm to L^2 is not straightforward, and, as discussed in [4], one can at best expect convergence at order $2m$. Moreover, the energy and L^2 error bounds derived in [4] degrade in time by factors of t^2 and t^3 respectively; we have never observed this growth in numerical experiments. However, it is observed in [4] that for m even the conservative approximation to the acoustic system leads to convergence at order $2m + 2$ and an argument is presented in one space dimension to explain it. The focus here is on methods with $m \geq 3$ and our experiments do not unambiguously determine if this phenomenon occurs, though least squares fits to the convergence rate for $m = 4$ do generally exceed 10. One experiment with $m = 2$ does very clearly exhibit convergence at order 6, and so we conjecture that the convergence rate is in fact $2m + 2$ for m even.

4 Numerical Experiments

Here we present some illustrations of the performance of the proposed methods for the transverse magnetic reduction of Maxwell's equations in two space dimensions. In all our examples we simply impose periodicity in space. We note that for these simple domains it is also straightforward to implement perfect electric conductor boundary conditions by imposing appropriate even and odd extensions of the electric fields at the

boundary. This would be a primitive version of the compatibility boundary condition method mentioned above.

4.1 Dielectric Medium

We evolve solutions of the form:

$$\begin{aligned} E_x &= -\frac{k}{\epsilon\omega} \sin(kx) \cos(ky) \cos(\omega t) \\ E_y &= \frac{k}{\epsilon\omega} \cos(kx) \sin(ky) \cos(\omega t) \\ H_z &= \sin(kx) \sin(ky) \sin(\omega t), \end{aligned}$$

with $(x, y) \in (-\pi, \pi)^2$, $\epsilon = \frac{5}{4}$, $\mu = \frac{4}{5}$, $\omega = \sqrt{2}k$. We present two sets of experiments. The first is simply to examine the convergence rates for various values of m . The second is to compare efficiency in terms of total degrees-of-freedom required as well as CPU time for problems of varying difficulty and error tolerances.

Convergence

We fix $k = 40$ and solve to $T = 100$. Since the wave speed is 1 and the wavelength is $2\pi/40$ a wave can travel approximately 636.6 wavelengths during the simulation and in time there are 900.3 periods. Here we vary m from 3 to 6 and sample with mesh sizes in convenient increments starting with meshes which produce errors roughly from 1% to 10%. Precisely for $m = 3$ we take $\Delta_x = \Delta_y = 2\pi/N_G$ with $N_G = 125 : 25 : 275$. For $m = 4$ we take $N_G = 100 : 25 : 250$, for $m = 5$ $N_G = 50 : 25 : 200$, and for $m = 6$ $N_G = 40 : 20 : 160$. In our comparisons we will always consider degrees-of-freedom per wavelength for each coordinate direction. As the number of degrees-of-freedom is $m + 1$ the ranges here begin with 12.5 for $m = 3, 4$, 7.5 for $m = 5$, and 7.0 for $m = 6$. In all cases we choose

$$\text{CFL} = \frac{\Delta t}{\Delta_x} = 0.9,$$

and use a temporal order $q = m + 2$. Recall that our stability proofs assume a much larger temporal order, $q = 3m + 2$, but our experiments show that $q = m + 2$ is sufficient for $m = 3 - 6$ and that increasing q does not improve accuracy. In some experiments below we use even higher values of m where we found that q needed to be $m + 3$ for stability with $\text{CFL} = 0.9$.

We approximate the L^2 error every time step by interpolating the Hermite solution onto a $2m \times 2m$ mesh in each cell and summing the results. Precisely we define the relative error

$$E^2(m, \Delta_x) = (4\sqrt{N_T})^{-1} \sum_{j=1}^{N_T} \|H_z^{\Delta_x}(t_j) - H_z(t_j)\|_{\ell^2}^2, \quad (57)$$

where N_T is the number of steps and $H_z^{\Delta_x}$ represents the interpolant of the Hermite solution onto the fine mesh. (Here we have used π as the relative scale since it is the

maximum L^2 -norm of H_z .) The results, shown in Figure 1, are sometimes choppy from mesh to mesh. We display a linear least squares fit to the log of the error as a function of the log of DOF/λ . This produces convergence rate estimates shown in Table 1. In all cases these meet or exceed the theoretical rate of $2m$. For the cases $m = 3 - 4$ they are in fact consistent with $2m + 2$, but we do not claim that these methods have a theoretical convergence rate greater than $2m$.

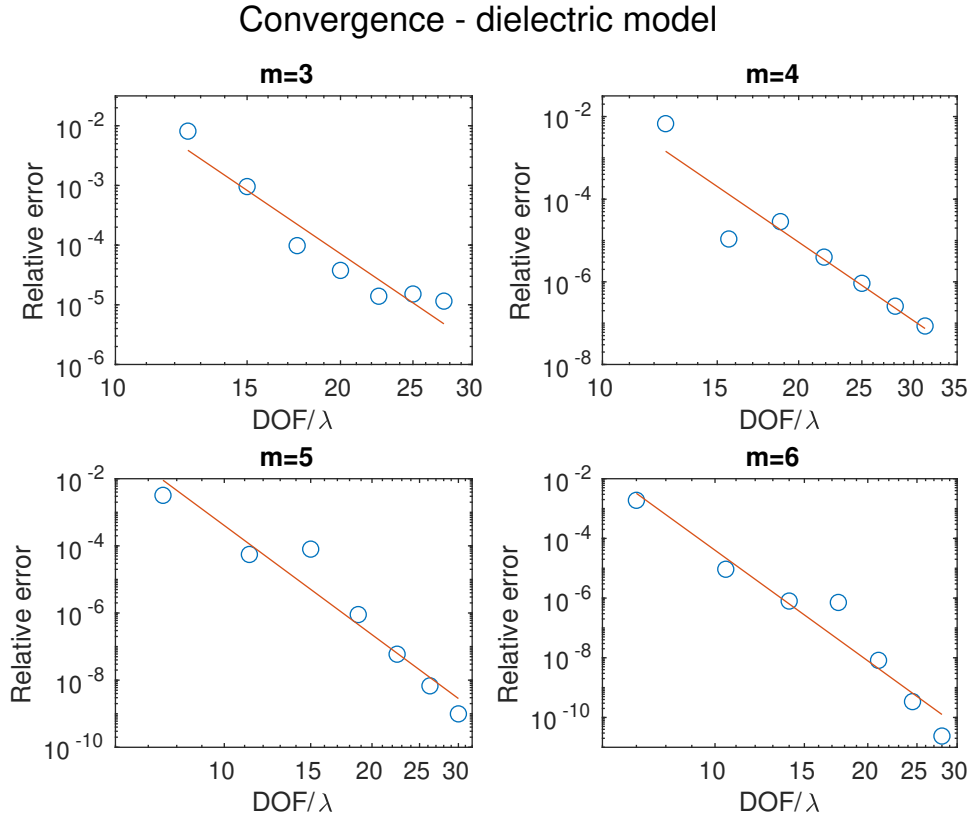


Fig. 1 Convergence for $m = 3 - 6$, $k = 40$, $T = 100$ in a dielectric medium. Errors are computed by comparing the Hermite interpolant of the numerical solution to the exact solution for each time step.

The convergence arising from the various choices for m is directly compared in Figure 2. The results in general show that for any particular error level the larger values of m are more efficient in terms of degrees-of-freedom required. We will further examine the efficiency question in detail for more challenging problems below.

Efficiency

Here we consider larger values of k , $k = 50, 100, 200$, still evolving to $T = 100$. Varying $\Delta_x = \Delta_y = \frac{2\pi}{N_G}$ by sampling N_G in increments of 5 we determine the coarsest mesh

m	DOF/ λ	Fit Rate
3	12.5 – 27.5	8.5
4	12.5 – 31.25	10.8
5	7.5 – 30	10.8
6	7 – 28	12.3

Table 1 Observed convergence for $m = 3 - 6$ with $k = 40$ and $T = 100$ for the dielectric medium. Here DOF/λ denotes the number of degrees-of-freedom per wavelength in each coordinate direction, $N_G(m+1)/k$ where the mesh is $N_G \times N_G$. That is $\Delta_x = \Delta_y = 2\pi/N_G$. The error is computed by (57).

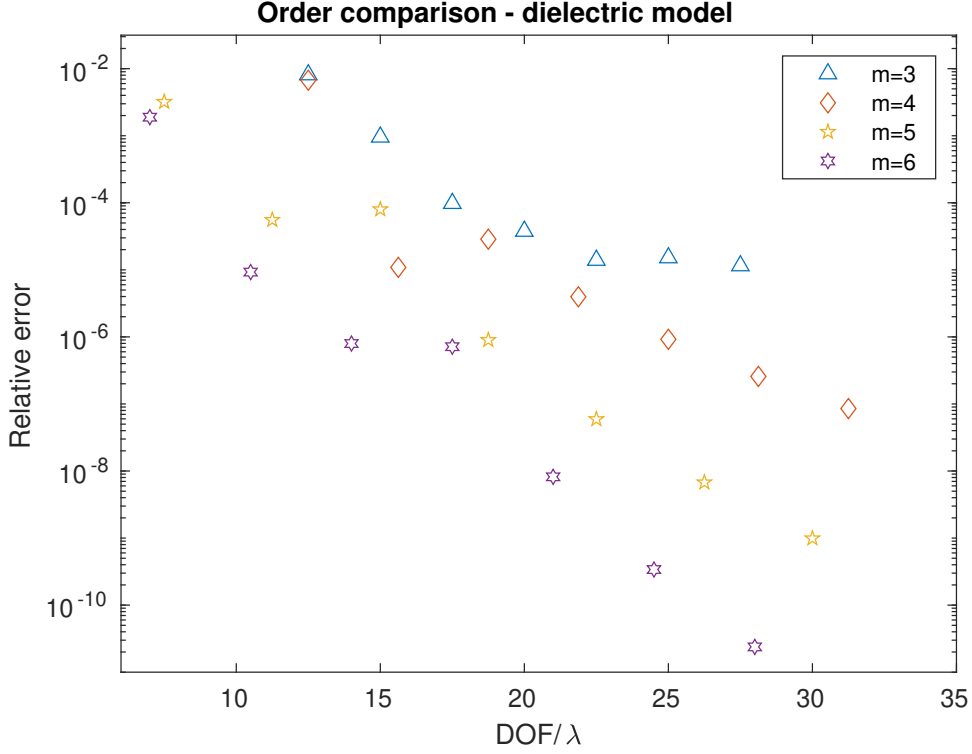


Fig. 2 Comparison of accuracy for $m = 3 - 6$, $k = 40$, $T = 100$ in the dielectric medium. Errors are computed by comparing the Hermite interpolant of the numerical solution to the exact solution for each time step.

for which the maximum recorded error relative to the maximum of the L^2 -norm of $H_z(\pi)$ is below the tolerances $\tau = 1\%$ and $\tau = 0.1\%$. Note that for these more challenging experiments waves propagate for approximately 796, 1592 and 3183 wavelengths, respectively, corresponding to approximately 1125, 2251, and 4502. temporal periods. As the problem difficulty increased we also increased the values of m tested to $m = 7$ and $m = 8$ as the lower order schemes became clearly less competitive. For these cases we needed to set $q = m + 3$ to maintain stability at $\text{CFL} = 0.9$. For comparison we also

tabulate the CPU times in seconds, which are obviously dependent on the implementation and hardware¹, and vary somewhat with repeated runs. Nonetheless we think the comparisons are still of interest. We remark that for the larger values of m the cell widths themselves were larger than a wavelength.

m	k	τ	L	DOF/ λ	Time	E_{\max}
3	50	$1e(-2)$	200	16.0	7.8(2)	8.1(-3)
4	50	$1e(-2)$	140	14.0	5.5(2)	8.5(-3)
5	50	$1e(-2)$	70	8.4	1.3(2)	6.0(-3)
6	50	$1e(-2)$	55	7.7	8.8(1)	2.5(-3)
3	50	$1e(-3)$	250	20.0	2.9(3)	7.3(-4)
4	50	$1e(-3)$	185	18.5	1.1(3)	6.8(-4)
5	50	$1e(-3)$	85	10.2	2.1(2)	3.0(-4)
6	50	$1e(-3)$	65	9.1	1.5(2)	3.8(-4)
5	100	$1e(-2)$	160	9.6	1.4(3)	1.5(-2)
6	100	$1e(-2)$	120	8.4	9.3(2)	9.7(-3)
7	100	$1e(-2)$	100	8.0	9.5(2)	3.9(-3)
5	100	$1e(-3)$	170	10.2	1.7(3)	6.6(-4)
6	100	$1e(-3)$	130	9.1	1.2(3)	7.9(-4)
7	100	$1e(-3)$	115	9.2	1.2(3)	3.8(-4)
6	200	$1e(-2)$	250	8.8	9.0(3)	6.2(-3)
7	200	$1e(-2)$	200	7.9	8.4(3)	7.9(-3)
8	200	$1e(-2)$	180	8.1	1.7(4)	5.5(-3)
6	200	$1e(-3)$	265	9.3	9.5(3)	2.8(-4)
7	200	$1e(-3)$	230	9.2	1.2(4)	7.5(-4)
8	200	$1e(-3)$	195	8.8	1.8(4)	5.3(-4)

Table 2 Values of N required for various values of m to achieve tolerances of 1% and 0.1% at $T = 100$ for various values of k .

The results, shown in Table 2, clearly illustrate the effectiveness of the high order methods and the small computational overhead for Hermite methods as m is increased. In all cases we achieve the desired tolerances with around 8 – 9 degrees of freedom per wavelength if we choose m large enough. Moreover, due to the the fact that we can choose the CFL number independent of m , the large m runs were often faster. Although we are cognizant of the pitfalls in the interpretation of timing data, we still believe that it is worth noting that in all but one case $m = 6$ achieved the tolerances in the least measured CPU time, and the increase in the number of degrees of freedom per wavelength is quite mild; for example for the 0.1% tolerance the $m = 6$ runs required 9.1, 9.1, and 9.3 as k was increased from 50 to 200.

¹We implemented the method in Fortran 90, compiling with *gfortran* and an optimization -O4. The hardware is a single Intel i9-13900H core with 64 GiB memory.

4.2 Dispersive Medium

As an example we consider a single-term Lorentz model for the permittivity and approximate solutions of the form considered in [15]. Specifically we take:

$$\epsilon = \mu = 1, \quad \Omega_{e,1} = 1, \quad \omega_{e,1} = \sqrt{1.052\pi} \approx 1.818, \quad \gamma_{e,1} = .0107,$$

which can be obtained by scaling the model for cubic silicon carbide listed in [16]. We will also carry out experiments for the Sellmeier model obtained by setting $\gamma_{e,1} = 0$.

Assuming 2π -periodicity we again take $k = 40$ and $T = 100$ and approximate solutions of the form

$$\begin{aligned} E_x &= -\frac{1}{2k} \sin(kx) \cos(ky) (\omega \cos(\omega t) - \theta \sin(\omega t)) e^{-\theta t}, \\ E_y &= \frac{1}{2k} \cos(kx) \sin(ky) (\omega \cos(\omega t) - \theta \sin(\omega t)) e^{-\theta t}, \\ H_z &= \sin(kx) \sin(ky) \sin(\omega t) e^{-\theta t}, \\ K_x &= \frac{1}{2k\omega_{e,1}^2} \sin(kx) \cos(ky) (-2\omega\theta \cos(\omega t) + (2k^2 + \theta^2 - \omega^2) \sin(\omega t)) e^{-\theta t}, \\ K_y &= -\frac{1}{2k\omega_{e,1}^2} \cos(kx) \sin(ky) (-2\omega\theta \cos(\omega t) + (2k^2 + \theta^2 - \omega^2) \sin(\omega t)) e^{-\theta t}, \\ L_x &= \frac{1}{2k\omega_{e,1}^2 (\theta^2 + \omega^2)} \sin(kx) \cos(ky) \\ &\quad \times ((\theta^2 + \omega^2 - 2k^2) \omega \cos(\omega t) - (2k^2 + \theta^2 + \omega^2) \theta \sin(\omega t)) e^{-\theta t}, \\ L_y &= -\frac{1}{2k\omega_{e,1}^2 (\theta^2 + \omega^2)} \cos(kx) \sin(ky) \\ &\quad \times ((\theta^2 + \omega^2 - 2k^2) \omega \cos(\omega t) - (2k^2 + \theta^2 + \omega^2) \theta \sin(\omega t)) e^{-\theta t}, \end{aligned}$$

where $z = -\theta + i\omega$ is a root of the quartic equation

$$z^4 + \gamma_{e,1} z^3 + (2k^2 + \omega_{e,1}^2 + \Omega_{e,1}^2) z^2 + 2k^2 \gamma_{e,1} z + 2k^2 \Omega_{e,1}^2 = 0.$$

For our choice of parameters we compute the roots (labelled r for resonant and h for high-frequency):

$$\theta_r = 0.005344476784229 \quad \omega_r = 0.999469550181686, \quad (58)$$

$$\theta_h = 0.000005523215771 \quad \omega_h = 56.597756028029032, \quad (59)$$

Setting $\gamma_{e,1} = 0$ we have $\theta = 0$ and

$$\omega_r^S = 0.999483839356918, \quad \omega_h^S = 56.597756029072784.. \quad (60)$$

For the Lorentz model $\Gamma_V = 0$ and so we need only evolve \tilde{D}_W satisfying

$$\frac{\partial \tilde{D}_W}{\partial t} = -\gamma_{e,1} \begin{pmatrix} K_x \\ K_y \end{pmatrix}. \quad (61)$$

The implicit Nordsieck method we use to evolve (61) employs polynomials of degree 6 which limits the formal method order to 6 in time. Nonetheless we will use values of m ranging from 2 to 6 to understand how the discretization of the dissipative term affects accuracy.

Obviously, the high-frequency solutions, H_z , of the Sellmeier model and the Lorentz model will be approximately equal up to $T = 100$; their maximum relative difference is approximately 5×10^{-4} . However, we will see that our method performs differently in these two cases.

4.3 Resonant Case

As in the dielectric case we test for convergence with m varying from 3 to 6. We fixed CFL = 0.9, which led to stable results for the meshes tested. The meshes were chosen to have errors around 1% for the coarsest mesh and the mesh sizes changed by a convenient factor. Precisely for $m = 3$ we use $N_G = 100 : 25 : 250$, for $m = 4$ $N_G = 50 : 25 : 200$, for $m = 5$ $N_G = 50 : 25 : 200$, and for $m = 6$ $N_G = 30 : 20 : 150$.

The results, shown in Figure 3, are again choppy from mesh to mesh. We display a linear least squares fit to the log of the error as a function of the log of DOF/ λ . This produces convergence rate estimates shown in Table 3. Perhaps surprisingly, in almost all cases these meet or exceed the theoretical rate of $2m$ for a dielectric medium or Sellmeier model, exceeding the theoretical rate of 6 of the approximation to the dissipative term in the Lorentz model. We suspect this is due the contrast between the spatial and temporal frequencies; even with CFL = 0.9 we are somewhat overresolved in time.

m	DOF/ λ	Fit Rate
3	10 – 25	7.3
4	6.25 – 25	11.0
5	7.5 – 30	12.4
6	5.25 – 26.25	10.5

Table 3 Observed convergence for $m = 3 - 6$ with $k = 40$ and $T = 100$ in the Lorentz model for the near-resonant mode. Here DOF/ λ denotes the number of degrees-of-freedom per wavelength in each coordinate direction, $N_G(m + 1)/k$ where the mesh is $N_G \times N_G$. That is $\Delta_x = \Delta_y = 2\pi/N_G$. The error is computed by (57).

The convergence arising from the various choices for m is directly compared in Figure 4. Again the results show that for any particular error level the larger values of m are generally more efficient in terms of degrees-of-freedom required.

Convergence - resonant mode

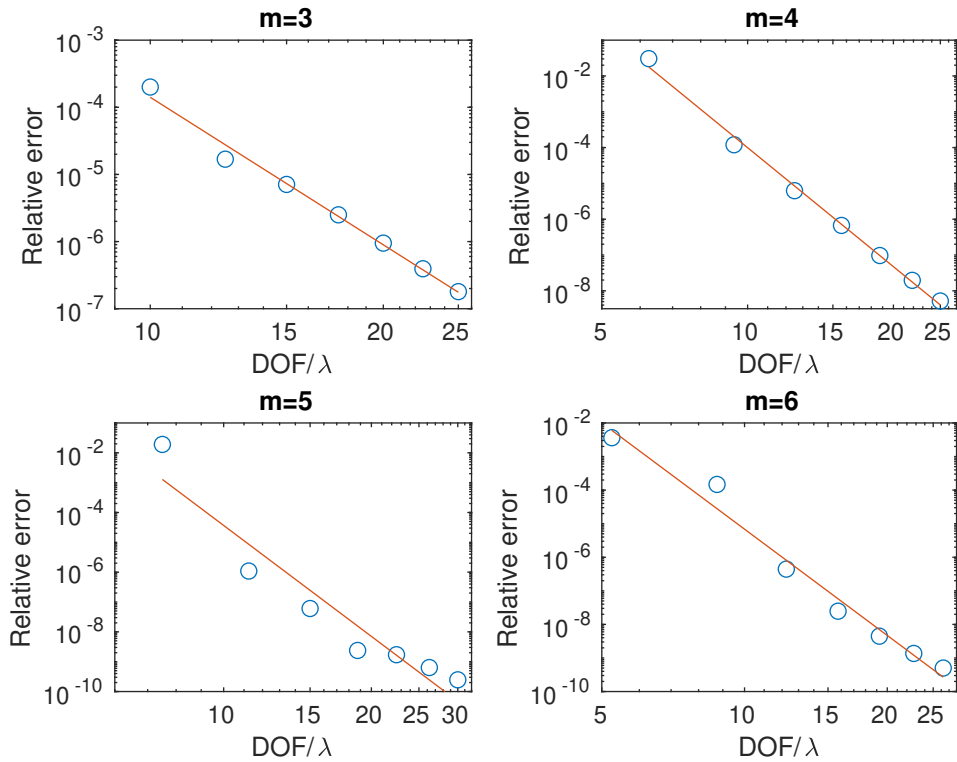


Fig. 3 Convergence for $m = 3-6$, $k = 40$, $T = 100$ for the near-resonant mode in a Lorentz medium. Errors are computed by comparing the Hermite interpolant of the numerical solution to the exact solution for each time step.

4.4 High-Frequency Case

We now consider the high-frequency solution of the Lorentz model with $k = 40$. Recall that the dissipation is nearly negligible in this case; the solution of the Sellmeier model obtained by setting $\gamma_{e,1} = 0$ agrees with the solution of the Lorentz model to more than three digits of accuracy, and so adding the dissipative term only improves accuracy if we solve with a tolerance below 10^{-4} . Nonetheless we find that the proposed method is limited by the sixth order treatment of the dissipative terms, and that nothing is gained by increasing m beyond 3. In addition, comparing the results with $m = 3$ for the Lorentz model to those shown below for the Sellmeier model we see that the mesh must be refined by more than 50% to achieve comparable accuracies.

In Figure 5 we examine convergence for $m = 2$ and $m = 3$. For $m = 2$ we vary N_G from 200 to 800 and clearly observe sixth order convergence; the least-squares fit produces an estimated rate of 6.2. For $m = 3$ we vary N_G from 150 to 450 but only observe convergence for $N_G \geq 300$. The least squares fit to the last three data points yields an estimated convergence rate of 7.5.

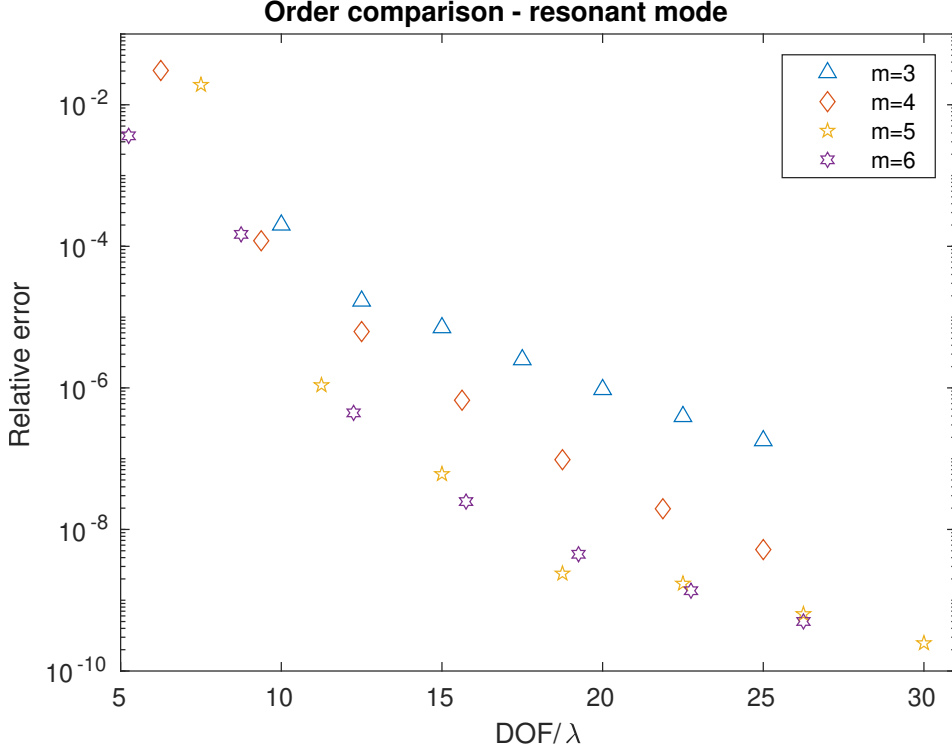


Fig. 4 Comparison of accuracy for $m = 3 - 6$, $k = 40$, $T = 100$ in the Lorentz medium for the near-resonant mode. Errors are computed by comparing the Hermite interpolant of the numerical solution to the exact solution for each time step.

The convergence arising for $m = 2 - 4$ is directly compared in Figure 6. We observe that of the three choices $m = 4$ is the least efficient in terms of degrees-of-freedom required for a given tolerance, though there is some advantage to choosing $m = 3$.

4.5 Sellmeier Model

Lastly we solve the Sellmeier model for the high-frequency mode. Here again we compare results for $m = 3 - 6$. The mesh sequences tested were $N_G = 150 : 25 : 300$ for $m = 3$, $100 : 25 : 250$ for $m = 4$, $50 : 25 : 200$ for $m = 5$, and $40 : 20 : 160$ for $m = 6$.

The results, shown in Figure 7, are very similar to the dielectric and resonant cases. The least squares fit convergence rates produces convergence rate estimates shown in Table 4. In all cases these are at least $2m$.

The convergence arising from the various choices for m is directly compared in Figure 8. Again the results show that for any particular error level the larger values of m are generally more efficient in terms of degrees-of-freedom required.

Convergence - high-frequency mode

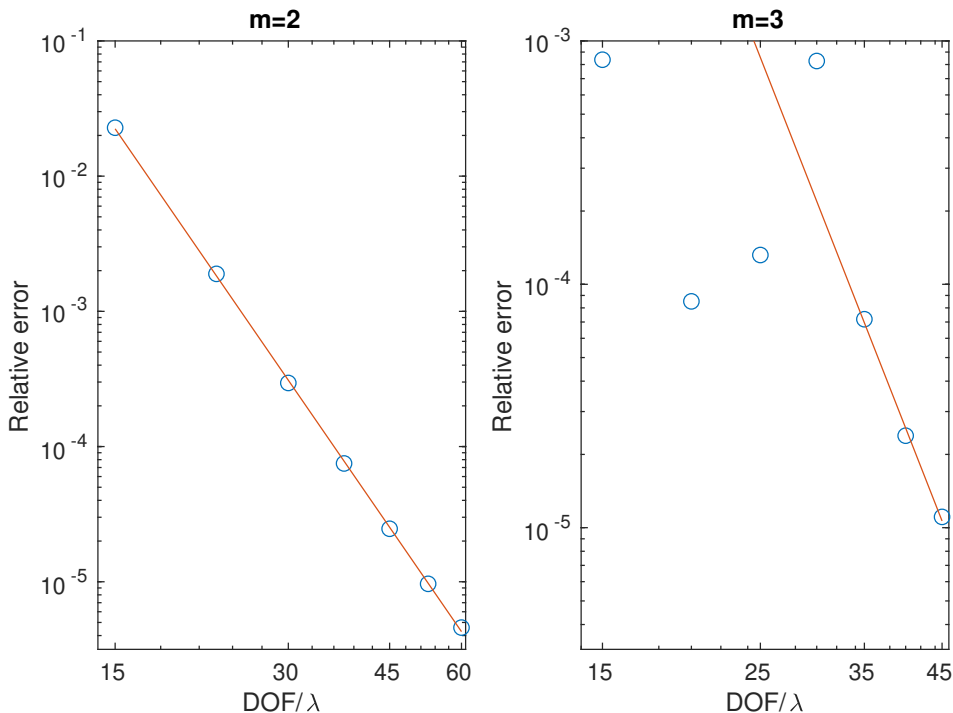


Fig. 5 Convergence for $m = 2 - 3$, $k = 40$, $T = 100$ for the high-frequency mode in a Lorentz medium. Errors are computed by comparing the Hermite interpolant of the numerical solution to the exact solution for each time step.

m	DOF/λ	Fit Rate
3	15 – 30	6.3
4	12.5 – 31.25	10.8
5	7.5 – 30	10.6
6	7 – 28	12.4

Table 4 Observed convergence for $m = 3 - 6$ with $k = 40$ and $T = 100$ for the Sellmeier model. Here DOF/λ denotes the number of degrees-of-freedom per wavelength in each coordinate direction, $N_G(m+1)/k$ where the mesh is $N_G \times N_G$. That is $\Delta_x = \Delta_y = 2\pi/N_G$. The error is computed by (57).

5 Conclusions and Open Issues

In conclusion we have proposed arbitrary-order energy-conserving Hermite discretizations of Maxwell’s equations for both dielectric and dissipation-free dispersive media. For these cases and with time-stepping of sufficiently high order we prove stability for $\frac{\Delta t}{|\Delta_x|} < 1$ independent of order. Numerical experiments show that the high-order schemes are capable of accurately propagating waves over thousands of wavelengths

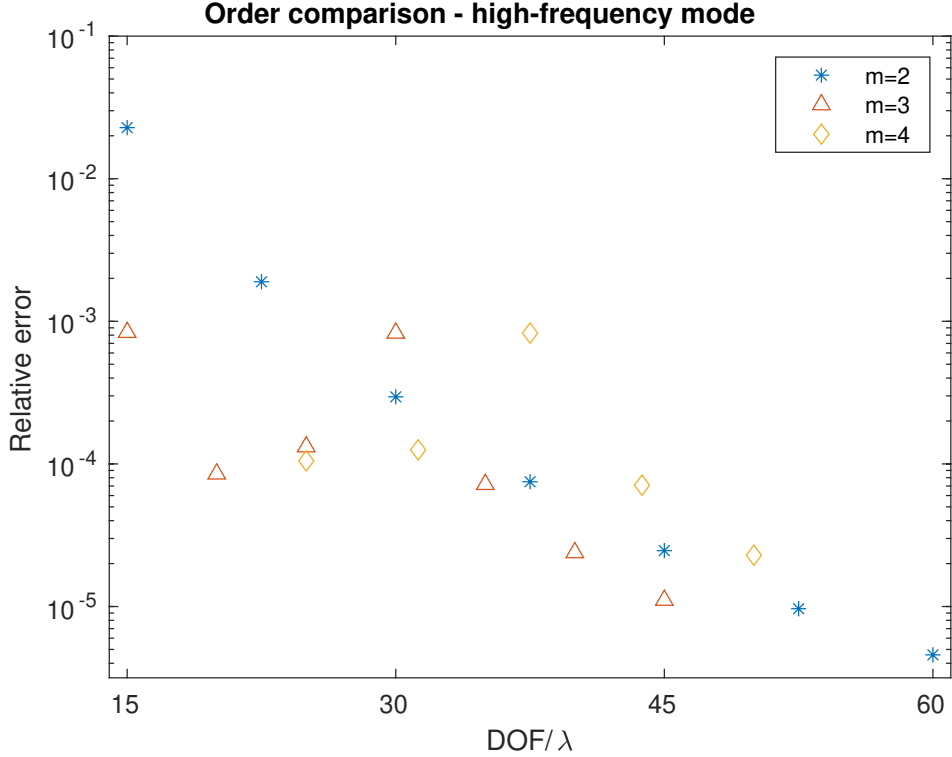


Fig. 6 Comparison of accuracy for $m = 2 - 4$, $k = 40$, $T = 100$ in the Lorentz medium for the high-frequency mode. Errors are computed by comparing the Hermite interpolant of the numerical solution to the exact solution for each time step.

with 9 or fewer degrees-of-freedom per wavelength. We also show how to include dissipation in the dispersive models, though this limits the formal order of accuracy and, in some cases, significantly degrades efficiency.

From a practical perspective, future work will focus on implementations in more complex geometry incorporating boundary and interface conditions and on exploiting the locality of the evolution formulas for efficient implementation on current computer architectures. We will also consider if the possibility of using high-order dissipative Hermite methods [2] is worthwhile for Lorentz models.

In terms of theory, the fundamental open issues are a complete analysis of convergence in L^2 and of the stability of the boundary and interface approximations.

Acknowledgments. This work was funded in part by National Science Foundation Grants DMS-2012296, DMS-2309687 and DMS-2210286. Any opinions, findings, and conclusions or recommendations expressed in this material are those of the authors and do not necessarily reflect the views of the NSF.

Convergence - Sellmeier model

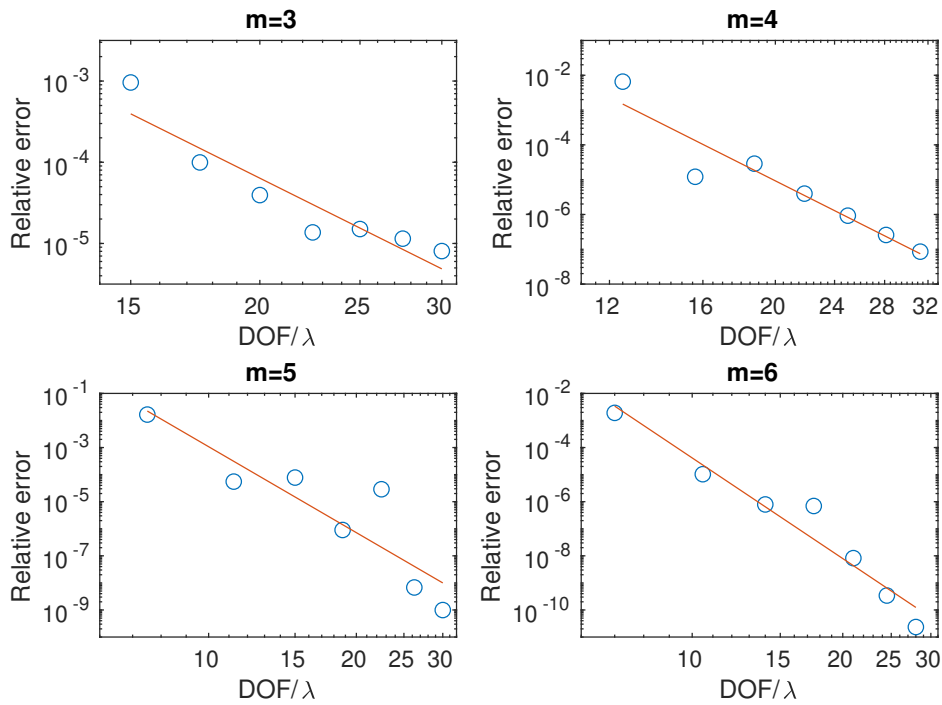


Fig. 7 Convergence for $m = 3 - 6$, $k = 40$, $T = 100$ for the Sellmeier model. Errors are computed by comparing the Hermite interpolant of the numerical solution to the exact solution for each time step.

Statements and Declarations

Competing Interests : The authors declare there are no competing interests.

Code Availability : The source codes used to produce the results in this paper are available by request to the corresponding author.

References

- [1] Appelö, D., Hagstrom, T.: Solving PDEs with Hermite interpolation. Lecture Notes in Computational Science, pp. 31–49. Springer, Cham (2015)
- [2] Goodrich, J., Hagstrom, T., Lorenz, J.: Hermite methods for hyperbolic initial-boundary value problems. *Math. Comp.* **75**, 595–630 (2006)
- [3] Appelö, D., Hagstrom, T., Vargas, A.: Hermite methods for the scalar wave equation. *SIAM J. Sci. Comput.* **40**, 3902–3927 (2018)
- [4] Vargas, A., Hagstrom, T., Chan, J., Warburton, T.: Leapfrog time-stepping for Hermite methods. *J. Sci. Comput.* **30**, 289–314 (2019)

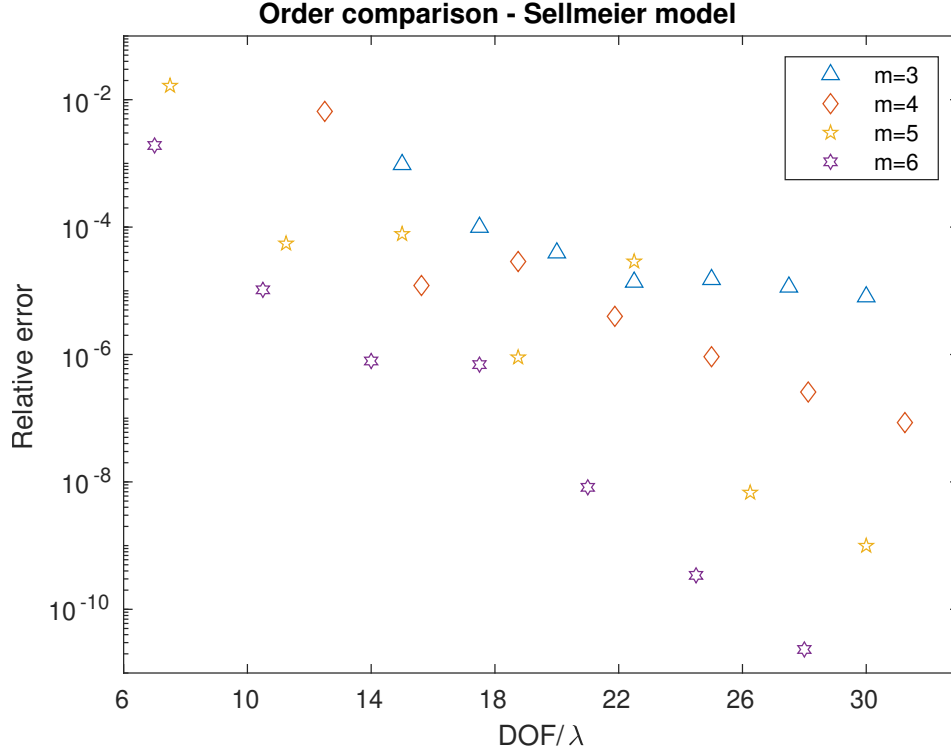


Fig. 8 Comparison of accuracy for $m = 3 - 6$, $k = 40$, $T = 100$ for the Sellmeier model. Errors are computed by comparing the Hermite interpolant of the numerical solution to the exact solution for each time step.

- [5] Vargas, A., Chan, J., Hagstrom, T., Warburton, T.: GPU acceleration of Hermite methods for simulation of wave propagation. *Lecture Notes in Computational Science*, pp. 357–368. Springer, Cham (2017)
- [6] Prokopeva, L., Borneman, J., Kildishev, A.: Optical dispersion models for time-domain modeling of metal-dielectric nanostructures. *IEEE Trans. on Magnetics* **47**, 1150–1153 (2011)
- [7] Law, Y.-M., Peng, Z., Appelö, D., Hagstrom, T.: A Hermite method for nonlinear dispersive media. In preparation (2023)
- [8] Law, Y.-M., Appelö, D., Hagstrom, T.: The Hermite-Taylor correction function method for embedded boundary and Maxwell’s interface problems. In preparation (2023)
- [9] Hairer, E., Norsett, S., Wanner, G.: *Solving Ordinary Differential Equations I, Nonstiff Problems*. Springer, New York (1992)

- [10] Loya, A., Appelö, D., Henshaw, W.: Hermite methods for the wave equation: Compatibility and interface conditions. In preparation (2023)
- [11] Holland, R.: Finite-difference solution of Maxwell's equations in generalized nonorthogonal coordinates. *IEEE Trans. Nuclear Sci.* **30**, 4589–4591 (1983)
- [12] Appelö, D., Chen, R., Hagstrom, T.: A hybrid Hermite-discontinuous Galerkin method for hyperbolic systems with applications to Maxwell's equations. *J. Comput. Phys.* **257**, 501–520 (2013)
- [13] Law, Y.-M., Appelö, D.: The Hermite-Taylor correction function method for Maxwell's equations. *Commun. Appl. Math. and Comp.* (2023) <https://doi.org/10.1007/s42967-023-00287-5>
- [14] Joly, P.: Variational methods for time-dependent wave propagation problems. In: Ainsworth, M., Davies, P., Duncan, D., Martin, P., Rynne, B. (eds.) *Topics in Computational Wave Propagation*, pp. 201–264. Springer, Berlin, Heidelberg (2003)
- [15] Bokil, V., Gibson, N.: Convergence analysis of Yee schemes for Maxwell's equations in Debye and Lorentz dispersive media. *Int. J. Numer. Anal. Mod.* **11**, 657–687 (2014)
- [16] Palik, E.D. (ed.): *Handbook of Optical Constants of Solids II*. Academic Press, San Diego (1998)